Geoderma 375 (2020) 114480

Contents lists available at ScienceDirect

Geoderma

journal homepage: www.elsevier.com/locate/geoderma

Effects of water, organic matter, and iron forms in mid-IR spectra of soils: Assessments from laboratory to satellite-simulated data

Nélida Elizabet Quiñonez Silvero[a], Luis Augusto Di Loreto Di Raimo[b], Gislaine Silva Pereira[c], Leonardo Pinto de Magalhães[c], Fabricio da Silva Terra[e], Marcos Augusto Ananias Dassan[c], Diego Fernando Urbina Salazar[d], José A.M. Demattê[a,*]

[a] Department of Soil, Luiz de Queiroz College of Agriculture, University of São Paulo, Piracicaba, Brazil
[b] College of Agronomy and Zootechnology, Federal University of Mato Grosso, Cuiabá, Brazil
[c] Department of Biosystems Engineering, Luiz de Queiroz College of Agriculture, University of São Paulo, Piracicaba, Brazil
[d] Université Paris-Saclay, INRAE, AgroParisTech, UMR ECOSYS, 78850 Thiverval-Grignon, France
[e] Institute of Agricultural Sciences, Federal University of Jequitinhonha and Mucuri Valleys, Brazil

ARTICLE INFO

Handling Editor: Morgan Cristine

Keywords:
Soil mineralogy
Spectroscopy
Thermal
ASTER
Soil attributes

ABSTRACT

The soil mineralogical constitution directly influences its chemical, physical and hydraulic characteristics. Although very important, it is still rarely used for decision-making in agriculture, mainly due to the complexity and cost of standard analyzes. In this sense, the middle infrared spectroscopy (mid-IR, 4000 to 400 cm^{-1}) has great potential to obtain soil mineralogical information quickly and accurately. Nevertheless, some soil constituents can severely influence the spectra and produce misinterpretations. In this research, we aim to detect changes in the mid-IR spectra caused by water, iron forms and organic matter (OM), and to relate soil attributes to laboratory spectra and remote sensing simulated spectral bands. The research area is located in São Paulo State, Brazil, where seventeen soil samples were collected. The reflectance intensities, shapes and absorption features of the mid-IR spectra before and after the removal of OM and iron forms and the addition of water were described. Soil attributes, such as kaolinite, gibbsite, 2:1 minerals among others were correlated with the mid-IR spectra and simulated ASTER spectral bands by Pearson's analysis, to verify its potential on mineralogical evaluation. The description of mid-IR revealed that the removal of the OM from the soil samples decreased the reflectance intensities between 4000 and 2000 cm^{-1}. Iron forms mainly influence the 3250 – 1200 cm^{-1} spectral range and mask the spectral features of other minerals as well. The addition of water masked several absorption features and decreased the reflectance intensities from 3700 to 2700 cm^{-1}. High correlation coefficients were obtained between soil attributes and ASTER simulated spectral bands, which allowed the selection of potential spectral regions for future satellite sensors: 2760 – 2500 cm^{-1} (3600 – 4000 nm), 2150 – 1875 cm^{-1} (4600 – 5300 nm), and 840 – 740 cm^{-1} (11900 – 3500 nm).

1. Introduction

Soil minerals have a strong influence on soil attributes and functions, such as charge dynamics, mechanical behaviors, water movement and nutrient cycling (Stenberg et al., 2010). Their study is essential for the evaluation and monitoring of soil conditions, which can also guide the implementation of better soil management activities. However, this information is still poorly used in decision-making practices, since the evaluation of soil mineralogy by traditional analyzes, such as X-ray diffraction and digestion procedures, have environmental, time and financial constraints (Robotti, 2013; Gholoubi et al., 2018; Bahia et al., 2015).

The reflectance spectroscopy has emerged as an alternative to obtain quick and reliable information about soil mineralogical composition (Soriano-Disla et al., 2014; Fang et al., 2018; Sun et al., 2018). Spectroscopy is related to the study of light interaction with matter, which is unique to a particular element or molecule and serves as a fingerprint for easy identification (Viscarra Rossel et al., 2006; Madejová et al., 2017). Such interactions take place across the entire electromagnetic spectrum and can be classified as electronic transitions in the visible (Vis: 400 – 700 nm), non-fundamental vibrations in the near-infrared (NIR: 700 – 1100 nm) and shortwave-infrared (SWIR:

* Corresponding author.
E-mail address: jamdemat@usp.br (J.A.M. Demattê).

https://doi.org/10.1016/j.geoderma.2020.114480
Received 13 December 2019; Received in revised form 7 May 2020; Accepted 24 May 2020

1100 – 2500 nm), and fundamental vibrations in the middle infrared (mid-IR: 2500 – 25000 nm, 4000 – 400 cm^{-1}) portions. The mid-IR comprises the thermal (TIR: 8000 – 14000 nm, 1250 – 714 cm^{-1}) and far-infrared (> 14000 nm, > 714 cm^{-1}) portions as well.

Several absorption features of soil minerals, such as those from hydroxyl and aluminol functional groups can be found in the Vis and NIR spectral ranges. Their main absorptions and other features are in the mid-IR portion. Even though the mid-IR spectra have great potential for soil mineralogical characterization (Janik et al., 2016), studies to understand and identify the most appropriate spectral features in this range for identifying clay minerals are still incipient in tropical soils for pedological assessments.

The interpretation of mid-IR data can be affected by several factors, such as organic matter (OM), water content, and particle size. These components can influence the spectral behavior of soil minerals by masking their absorption features or reducing reflectance intensities (Salisbury and Eastes, 1985; Stumpe et al., 2011; Janik et al., 2016). The indicated components can have even greater influence if the measurements are made via remote sensing, as we cannot control them. To understand and overcome these issues, spectral analysis before and after successive removals of soil components, and the influence of water by moistening and drying processes have been addressed in some works. In Australia, Yeasmin et al. (2017) tested different chemical treatments to remove the effects of organic matter in soil mid-IR spectra. They observed that the absorption features of iron and aluminum oxides (goethite and gibbsite, respectively) were affected by strong chemical removal treatments. Laub et al. (2019) studied the soil water influence by moistening and drying processes. The authors observed that the increase in drying temperature from 32° C to 105° C reduced the O–H absorption feature by 2%. A decrease in reflectance values across the spectra was observed as well. The soil moisture loss could be recovered by air humidity and therefore the influence of water content on mid-IR spectra could be more difficult to assess (Laub et al., 2019).

Further research is still needed to understand the entire spectral range of mid-IR and the influence of the factors mentioned. A detailed study of the influence of these factors can assist in the calibration of satellites. The Advanced Spaceborne Thermal Emission and Reflection Radiometer (ASTER), for example, has five spectral bands in the region of thermal infrared. Its importance for soil mineralogy and lithological evaluations has been highlighted in several works (Abrams and Yamaguchi, 2019; Bhadra et al., 2013; Cudahy et al., 2016; Kurata and Yamaguchi, 2019; Laukamp et al., 2012; Vicente and de Souza Filho, 2011; Mulder et al., 2013; Ninomiya and Fu, 2019). Besides that, other spectral ranges in the mid-IR region can also provide valuable information for soil mineralogical studies and need to be explored.

In this research, we aim to evaluate the influence of OM, iron forms (amorphous and crystalline) and water content in the mid-IR spectra (in laboratory and simulated ASTER thermal bands) of tropical soils. We also aimed to propose spectral ranges in the mid-IR region that have potential to assist forthcoming aerial and orbital sensors.

2. Material and methods

2.1. Study site characterization

We used a soil dataset containing 17 soil samples from three municipalities in São Paulo state (Lençóis Paulista, Macatuba, and Bauru), Brazil. This region is characterized by several sandstone and basalt formations, with wide variability in soil texture and soil classes. Surface soil samples (A horizon, 0 – 20 cm depth), were collected in soil profiles classified as: Rhodic Hapludox, Typic Hapludox, Typic Quartzipsamments, and Typic Paleudalf (Soil Survey Staff, 2014). Fig. 1 presents the flowchart of the methodological procedures of this study.

2.2. Laboratory analyses and treatments

The soil samples were air-dried, sieved through 2 mm and then analyzed in the laboratory. The organic matter content (OM) was determined following the Walkley-Black oxidation method (Walkley and Black, 1934).The particle size distribution (clay, sand, and silt contents) was determined by the pipette method, using sodium hydroxide as a dispersant agent (Teixeira et al., 2017). The sulfuric digestion was performed following the methodology described in EMBRAPA (1997), in which the soil samples were digested with sulfuric acid to obtain contents of total iron (Fe_2O_3), aluminum (Al_2O_3) and silicon oxides (SiO_2). The weathering indices Ki (SiO_2/Al_2O_3) and Kr [$SiO_2/(Al_2O_3 + Fe_2O_3)$] were calculated using these oxides contents. Amorphous iron was determined by extraction with acidic ammonium oxalate solution (McKeague and Day, 1965), and crystalline iron was determined by sodium dithionite-citrate-bicarbonate method (Holmgren, 1967). Kaolinite (Kt) and Gibbsite (Gb) was determined by differential thermal analysis (McKeague and Day, 1965) and Si + Al amorphous material by selective dissolution with boiled 0.5 N KOH. The 2:1 minerals content (V + M) was determined by the difference among the contents of iron, kaolinite, gibbsite, amorphous material and the total soil samples [(Fe_2O_3 + Kt + Gb + (Si + Al)) – total soil sample)]. More details about the methods used for laboratory analyzes was described in Demattê et al. (2007).

After the chemical and mineralogical analysis, the soil samples were submitted to three successive removal treatments. The first treatment consisted of removing the OM from the soil samples with 40 mL of H_2O_2 30% (T1-OM). In the second treatment, besides the OM, the amorphous iron was also removed using ammonium oxalate (T2-FeOX). Finally, the third treatment consisted of removing OM, amorphous iron and crystalline iron, the latter using dithionite-citrate-sodium bicarbonate (T3-FeD). The methods of iron extractions are described in Jackson (1969).

2.3. Mid-IR analysis and moisture influence

For mid-IR analysis, the soil samples were ground to obtain particles smaller than 100 mesh. Reflectance spectra were obtained with the Alpha Sample Compartment RT-DLaTGS ZnSe (Bruker Optik GmbH) equipped with an accessory for acquiring diffuse reflectance (DRIFT). The sensor has a HeNe laser positioned inside the equipment and a calibration pattern for each wavelength. It has a KBr beam, allowing a high amplitude of the incident radiance to penetrate the sample. Spectra were acquired between 4000 and 400 cm^{-1} (2500 – 25000 nm), with a spectral resolution of 2 cm^{-1} and 32 scans per minute per spectra. The reflectance values from 500 to 400 cm^{-1} (20000–25000 nm) were removed due to the low signal to noise ratios. A gold reference plate was used as standard, and the sensor was calibrated every four measurements.

The influence of soil water content in spectra was studied by wetting and drying processes. The wetting process consisted of sequentially adding three volumes of pure water (0.1, 0.2, and 0.3 mL) to the seventeen soil samples. One gram (1 g) of sieved soil (100 mesh) was placed in a Petri dish, and then the water was added, which was mixed with the soil to obtain a homogeneous sample for spectral analysis. Besides that, the soil samples were oven-dried in two temperatures (45 °C and 105 °C) for 24 h, and their spectra were measured before and after the drying processes, to show if the most adsorbed water could affect the spectra behaviors.

2.4. Statistical analysis of soil attributes and spectral behaviors

The chemical, physical, and mineralogical attributes were submitted to descriptive statistics. Pearson's correlation analysis was performed between laboratory's reflectance spectra and soil mineralogical constituents, to identify major diagnostic spectral features along the mid-IR range. In order to make the spectral descriptions easier, only the two

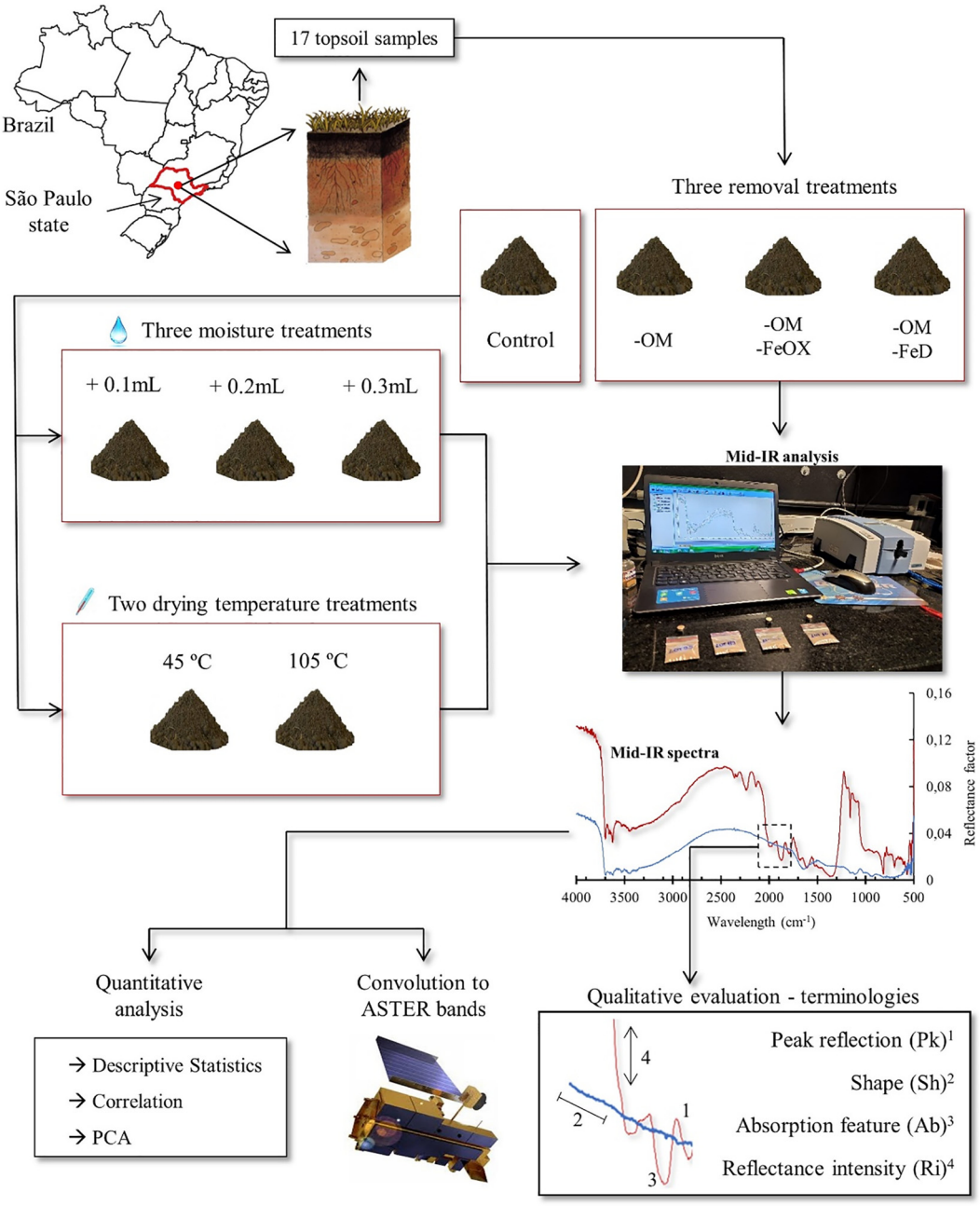

Fig. 1. Flowchart of the methodological procedures at different soil samples in this study. Treatments are represented by the following letters: Control: Control samples, -OM: organic matter removal, -FeOX: amorphous iron removal and -FeD: crystalline iron removal.

most textural contrasting soil samples (Rhodic Hapludox and Typic Quartzipsamment) were used to identify spectral alterations after the treatments. The following expressions were used to qualitatively describe the spectra: reflectance intensity (all reflectances along the spectral range without taking into account features and peaks - albedo); absorption feature (absorption in the curve, a negative valley - depression); reflection peak (positive and narrow reflectance as a peak); shape (format or specific behavior). These expressions corresponds to the MIRS (Multiple Interpretation of Reflectance Spectra), established by Demattê et al. (2014). Besides that, the Principal Component Analysis (PCA) was individually carried out in these two soils to reduce the spectral data dimensionality and to visualize their distribution patterns, in order to make possible the identification of clusters or distinguishing samples that received different chemical treatments.

2.5. ASTER satellite convolution and band position selection

The mid-IR spectra of the Rhodic Hapludox and Typic Quartzipsamment were convoluted to the five thermal bands (8000 – 12000 nm, 1250 – 714 cm^{-1}) of the Advanced Spaceborne Thermal Emission and Reflection Radiometer (ASTER). In the TIR range, all bodies with a temperature above absolute zero emit energy, known as emissivity (Wille et al., 2015). The ASTER sensor has five bands (bands 10, 11, 12, 13, and 14), with spectral ranges between 1235 and 1180 cm^{-1} (8125 – 8475 nm), 1180–1133 cm^{-1} (8475 – 8825 nm), 1120 – 1078 cm^{-1} (8925 – 9275 nm), 976 – 913 cm^{-1} (10250 – 10950 nm) and 913 – 858 cm^{-1} (10950 – 11650 nm) respectively (Tsu et al., 1996). The convolution analysis was performed in the R software (R Core Team, 2019), where a data frame with the spectral responses of each ASTER band (minimum and maximum described above) was built.

Table 1
Chemical and mineralogical analysis of soil samples.

Soil	*OM	Sand	Silt	Clay	SiO_2	Al_2O_3	TiO_2	MnO	Fe_2O_3	FeD	FeOX	Kt	Gb	V + M	Si + Al	Ki	Kr
Classes	g kg $^{-1}$																
RH	21	30	100	870	244.1	225.7	55.7	1.1	221.0	153.0	64.0	365.0	191.0	104.0	57.0	1.83	1.13
TH2	13	760	40	200	36.0	73.9	16.4	0.3	37.0	36.0	11.0	88.0	50.0	24.0	2.0	0.83	0.63
TH2	10	580	60	360	86.9	105.5	37.0	0.7	83.0	81.0	27.0	220.0	36.0	18.0	5.0	1.40	0.93
TH1	19	420	130	450	150.5	120.9	46.0	1.3	122.0	120.0	44.0	252.0	45.0	22.0	11.0	2.11	1.28
TH1	16	330	120	550	189.9	159.5	46.6	1.0	136.0	132.0	53.0	324.0	44.0	27.0	23.0	2.02	1.30
TH2	12	760	40	200	50.0	66.2	12.5	0.1	29.0	19.0	10.0	108.0	16.0	14.0	37.0	1.28	1.06
TE	15	310	120	570	181.8	193.6	59.9	1.1	197.4	151.0	80.0	285.0	91.0	46.0	3.0	1.60	0.99
TH2	21	680	80	240	66.0	67.3	56.3	0.5	86.0	53.0	36.0	132.0	12.0	12.0	31.0	1.66	1.08
TH2	16	620	40	340	67.0	86.6	31.2	0.5	83.0	79.0	27.0	207.0	17.0	17.0	20.0	1.32	0.82
TE	19	150	120	730	239.4	216.2	70.1	1.2	253.5	142.0	54.0	452.0	87.0	36.0	13.0	1.88	1.08
RH	13	610	120	270	39.5	46.2	32.6	0.8	81.0	75.0	17.0	140.0	11.0	14.0	30.0	1.45	0.68
RH	10	570	100	330	93.9	97.7	34.5	0.7	96.0	95.0	22.0	162.0	26.0	16.0	31.0	1.63	1.0
TH1	20	300	130	570	149.5	164.3	38.9	0.7	159.0	137.0	49.0	319.0	57.0	28.0	29.0	1.55	1.0
TQ	14	810	70	120	53.0	43.3	8.7	0.1	12.0	10.0	3.0	66.0	18.0	8.0	18.0	2.08	1.79
TP	9	850	40	110	100.0	71.9	18.7	0.3	44.0	41.0	8.0	134.0	22.0	22.0	1.0	2.36	1.69
TP	9	660	100	240	70.0	63.7	28.9	0.4	20.0	51.0	14.0	125.0	48.0	12.0	4.0	1.87	1.55
TQ	10	860	60	80	25.0	25.0	6.0	0.2	7.0	7.0	2.0	49.0	12.0	4.0	8.0	1.70	1.44

*OM: organic matter; Ki and Kr: weathering index; FeD: iron extracted by dithionite, FeOX: iron extracted by ammonium oxalate; Kt: kaolinite; Gb: gibbsite, V + M: vermiculite and mica; Si + Al: amorphous silicon and aluminum. RH: Rhodic Hapludox; TH1: Typic Hapludox (clay > 350 g kg^{-1}), TH2: Typic Hapludox (220 < clay < 250 kg g^{-1}); TH3: Typic Hapludox (150 < clay < 220 g kg^{-1}); TE: Typic Eutrustox; TP: Typic Paleudalf; TQ: Typic Quartzpament

For each spectral range, the median reflectance was calculated. The median reflectances were correlated to soil attributes by Pearson's analysis.

The potential spectral ranges was selected considering the correlation coefficients between soil attributes and the laboratory' mid-IR spectra (higher and lower than 0.8 and −0.8, respectively). The coincidence with atmospheric windows and radiative flux were also considered.

3. Results and discussions

3.1. Descriptive analysis of soil attributes

In Table 1 are shown the soil chemical, physical and mineralogical analyzes of the seventeen soil samples. The samples presented a wide variability in textural classes, from very sandy to clay soil (Fig. 2). The soil particle distribution's values varied from 80 to 870 g kg^{-1} and from 30 to 860 g kg^{-1} for clay and sand contents, respectively (Table 1). Soil attributes such as OM, 2:1 minerals (V + M), Si + Al, FeOX, TiO_2, and Gb had lower values with homogeneous distributions (Fig. 3). In contrast, the FeD, Fe_2O_3, Al_2O_3, SiO_2, and Kt contents presented a high variability, with values ranging from 7 to 221 g kg^{-1} (Table 1).

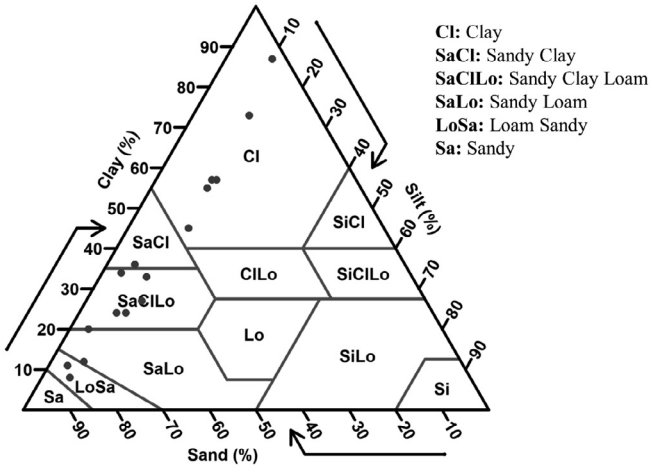

Fig. 2. Soil textural distribution plot.

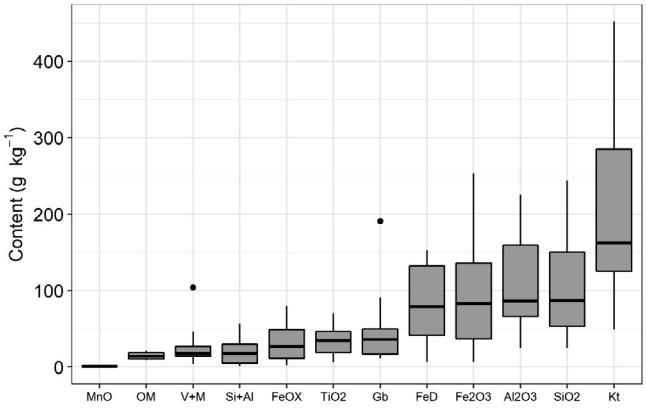

Fig. 3. Boxplot of the mineralogical analyzes. The following acronyms represent soil minerals and treatments: MnO: manganese dioxide, OM: organic matter, V + M: vermiculite + micas, Si + Al: amorphous silicon and aluminum, FeOX: amorphous iron extracted by ammonium oxalate, TiO_2: titanium dioxide, Gb: Gibbsite, FeD: crystalline iron extracted by dithionite, Fe_2O_3: total iron, Al_2O_3: aluminum oxide, SiO_2: silicon oxide and Kt: kaolinite.

Kaolinite is considered the most common mineral in the clay fraction of tropical soils (Schaefer et al., 2008). This 1:1 phyllosilicate plays a key role in soil structure and stability (Chen et al., 2000), and can severely affect the soil susceptibility to compaction (Smalley and Cabrera, 1969). The TiO_2 is present in these soils in values below 100 g kg^{-1} (Table 1 and Fig. 3), which are highly above those values described for highly weathered tropical soils (Smalley and Cabrera, 1969).

The variability observed in the distributions of soil attributes and textural classes are mainly explained by the differences in the contents of 1:1 phyllosilicates (Kt), iron oxides (hematite and goethite) and quartz of each soil type. For example, Rhodic Hapludox is characterized by having a clay or very clay texture (clay content > 350 g kg^{-1}) (Santos et al., 2013). Samples of the Rhodic Hapludox reached values up to 641.60 g kg^{-1} (Table 1). Typic Quartzipsamment is characterized by having 15% of clay and the predominance of quartz sand in the entire profile (Santos et al., 2013). Highly weathered soils, such as Rhodic Hapludox, Typic Hapludox and Typic Paleudalf, are characterized by having lower values of Ki and Kr indexes and, consequently, higher kaolinite, gibbsite and iron oxides (crystalline iron) contents

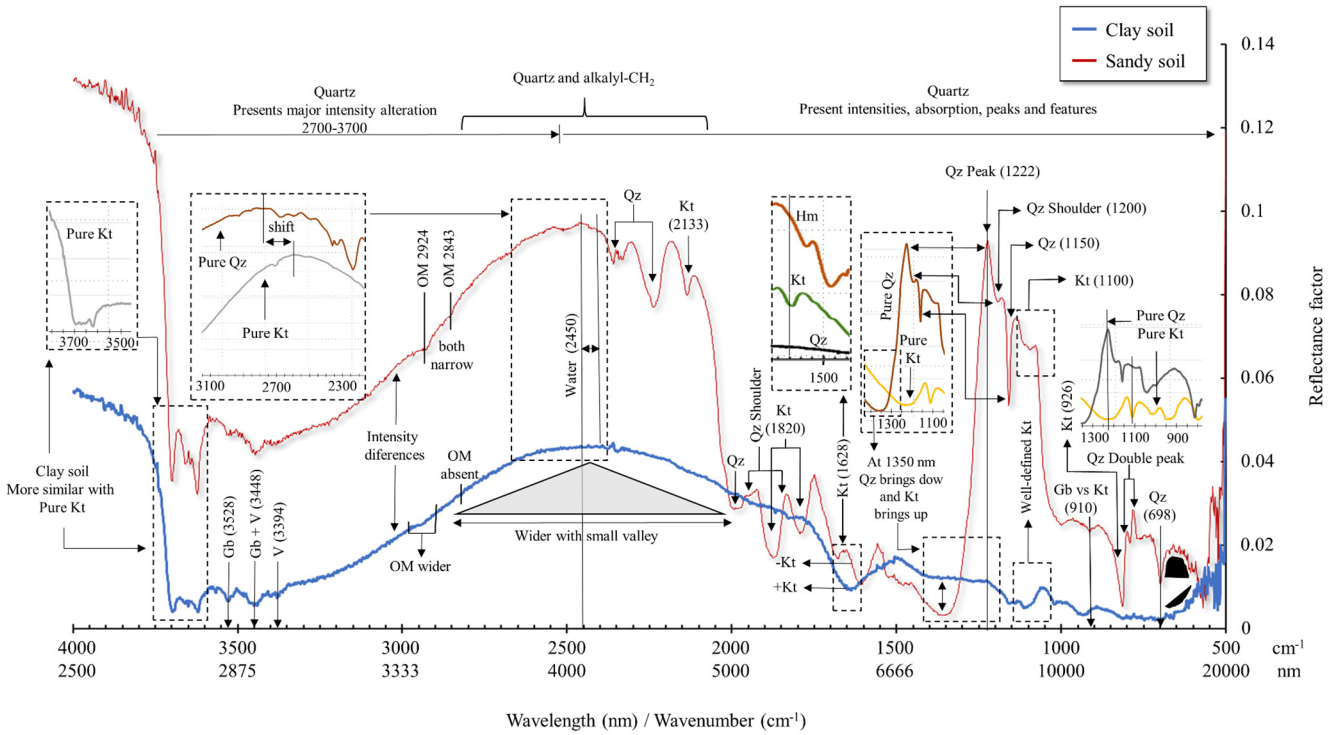

Fig. 4. Comparison between mid-IR spectra of clay (Rhodic Hapludox) and sandy (Typic Quartzpament) soil control samples. Soil minerals and components are represented by the following acronyms: Gb: gibbsite, Hm: Hematite, Kt: kaolinite, OM: organic matter, Qz: quartz, V: vermiculite + micas.

(Table 1).

3.2. Soil spectra description

The mid-IR spectral behaviors of the Rhodic Hapludox and Typic Quartzipsamment were very different (Fig. 4), where the sandy soil had greater reflectance intensities compared to the clay one over almost the entire spectrum. The spectral behavior was reversed in the following specific ranges: from 2020 cm^{-1} to 1960 cm^{-1}, from 1920 cm^{-1} to 1850 cm^{-1}, from 1810 cm^{-1} to 1775 cm^{-1} and from 1540 cm^{-1} to 1310 cm^{-1}.

The absorption features related to the bonds between hydroxyl and aluminum (Al-OH) (at 3695 cm^{-1}, 3653 cm^{-1} and 3622 cm^{-1}, for 1:1 and 2:1 phyllosilicates; at 3529 cm^{-1} for gibbsite; and at 3394 cm^{-1} for vermiculite) and iron (Fe-OH) (at 3448 cm^{-1} for goethite) were observed in both spectra (Fig. 4). Farmer (1968), White and Roth (1986), and Madejová (2003) also described the absorption features mentioned above. The first three features (3695 cm^{-1}, 3653 cm^{-1}, and 3622 cm^{-1}) were deeper for the clay soil, suggesting the predominance of 2:1 minerals (mica group). The remained absorption features presented the same behavior in the clay soil, but had greater amounts of 1:1 mineral (kaolinite), gibbsite, goethite and vermiculite. This information can be confirmed by the values in Table 1.

From 2500 to 500 cm^{-1}, the quartz had a great influence on the spectral intensity, with characteristic absorption features, reflection peaks, and other specific forms due to the interaction of radiation with Si-O bonds, clearly observed in the sandy soil (Fig. 4). Fundamental stretching of Si-O appeared at 2233 cm^{-1}, 2133 cm^{-1}, 1999 cm^{-1}, 1792 cm^{-1}, 1607 cm^{-1} and 1350 cm^{-1} (Salisbury, 1988), but was absent in the clay soil spectrum. Well-defined quartz reflection peak was indicated at 1222 cm^{-1}, due to the stretching of the Si-O, also known as the reststrahlen band (Thomson and Salisbury, 1993). A shoulder at 1190 cm^{-1} and a well-defined absorption at 1150 cm^{-1} were also highlighted. A double reflection peak at 797 and 778 cm^{-1} also appeared due to the quartz. The features mentioned were related to the pure quartz spectra highlighted in Fig. 4.

Kaolinite' absorption features observed in the clay soil were related to its predominance and quantity (Table 1). In fact, absorption features at 1630 cm^{-1}, 1125 cm^{-1} and 1025 cm^{-1} appeared broader and well-defined in the clay soil, and very narrow and less defined in the sandy (Fig. 4). Absorptions at 1945 cm^{-1} and 1820 cm^{-1} were attributed to phyllosilicates and were not observed in the clay spectrum, probably masked by iron oxides. Absorption features at the same position (specifically at 1100 cm^{-1}) were shown in the pure kaolinite and quartz spectra (Fig. 4). Both minerals (quartz and kaolinite) are silicates and have Si-O in their structures (Salisbury, 1988; Salisbury and D'Aria, 1992), which can be responsible for this feature. Depending on the concentration of each mineral in the soil, one can mask the other. For example, the sandy soil showed a less defined absorption feature at 1100 cm^{-1}, which was due to the quartz. Conversely, in the clay soil, the same absorption feature appeared well-defined due that the kaolinite content was higher than in the sandy soil.

Another important difference between mid-IR spectra of the clay and sandy soils (Fig. 4) was the shape around 1110 cm^{-1}. The clay soil presented a shape (from the peak to the valley) most similar to pure kaolinite than to quartz. The absorption at 698 cm^{-1} was present in the sandy soil and absent in the clay (Fig. 4). Despite this, at the end of the mid-IR spectra, there is a particular shape that differentiate sandy from clayey soils. The shape around 650 cm^{-1} goes from concave (sandy) to convex (clayey) (Fig. 4). This is due to a double effect where quartz brings spectra up (sandy) and greater amounts of kaolinite and gibbsite brings spectra down (clayey), creating the convexity shape.

Regarding the OM, subtle absorptions at 2924 and 2843 cm^{-1} were identified only in the sandy soil (Fig. 4), despite its lower OM content (Table 1). However, a wider shaped valley surrounding 2924 cm^{-1} was observed in the clay soil. These features have been assigned to alkyl-CH2 groups present in the OM (Salazar et al., 2020). McDowell et al. (2012) stated that absorption features observed in the mid-IR region could be related to organic molecules and some phosphorus and sulfur compounds. The OM in the soil consists mainly of poly-aromatic and

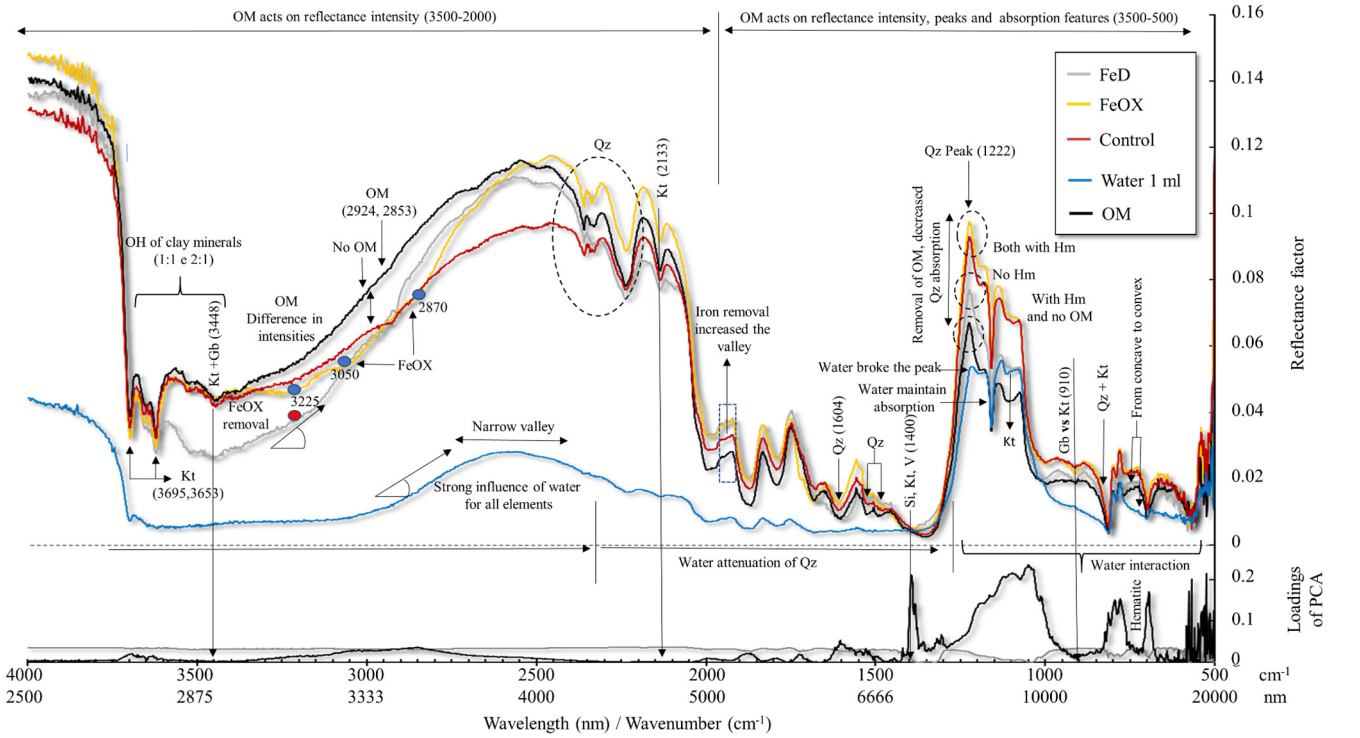

Fig. 5. Mid-IR spectra and PCA loadings of the sandy soil (Typic Quartzpament). Control and removal treatments: OM, crystalline iron (FeD) and amorphous iron (FeOX) removals and spectra with addition of water (1 mL). Soil minerals and components are represented by the following acronyms: Gb: gibbsite, Hm: Hematite, Kt: kaolinite, OM: organic matter, Qz: quartz, Si: Silicon, V: vermiculite + micas.

aliphatic acids, amides, esters and sugars and the combined action of these compounds have absorption features at 3400 cm^{-1}, 1600 cm^{-1}, 1400 cm^{-1} (Nguyen et al., 1991; Ziechmann, 1964) and at 2930 cm^{-1} and 2850 cm^{-1} (Viscarra Rossel et al., 2006). The abovementioned absorption features described in the literature were not observed here. It could probably due to the low OM content (< 2%) in both soils, which led to a less influence on the mid-IR spectra.

3.3. Effects of water content

Although three moisture levels (0.1 mL, 0.2 mL and 0.3 mL) and two drying temperatures (45 °C and 105 °C) were evaluated, only the spectra of both soils that received 0.1 mL of water are presented (Figs. 5 and 6). The mid-IR spectra of the soil samples that received larger amounts of water (0.2 and 0.3 mL) showed considerable noise, making comparison with the control samples difficult. The spectral noise probably resulted from the lack of soil matrix homogeneity, to which the equipment is extremely sensitive (Niemeyer et al., 1992). Besides that, there were no differences between the mid-IR spectra before and after the drying treatment. Probably, the amount of water adsorbed on the soil particles was insufficient to produce changes in the spectra.

The addition of water had a more prominent influence on the sandy soil's spectral behavior between the 4000 – 1400 cm^{-1}, in which the reflectance intensities decreased considerably (Fig. 5). The valley in the sandy that received the addition of water starts about 3000 cm^{-1} while in the control sample it starts at 3350 cm^{-1}. The presence of structural water in the soil could be related to this behavior (Salisbury, 1987). When water is not part of the mineral structure, it can form hydrogen bonds with other water molecules, resulting in a wide spectral band caused by the O–H stretching, which was observed in the soil that received the water treatment (0.1 mL).

The water added to the sandy soil masked most of the quartz's absorption features between 2500 and 1500 cm^{-1} (Fig. 5). The quartz reflection peak between 1222 and 1050 cm^{-1} decreased considerably and had its sharpness modified, although the absorption feature at 1155 cm^{-1} was maintained. Besides that, the absorption feature related to the Si-O symmetric stretching mode at the 833 cm^{-1} and 740 cm^{-1}, was less evident after the addition of water. The phyllosilicate's absorption features in the sandy soil related to 2:1 and 1:1 minerals were completely masked between 3695 cm^{-1} and 3394 cm^{-1}. White and Roth (1986) observed kaolinite' features in the spectral region mentioned as well.

The changes in the clay soil's mid-IR spectrum due to the addition of water were minimal compared to the sandy (Fig. 5). The wet clay soil showed almost the same spectral behavior than that of the dry one (control sample), although a slightly decrease in the reflectance intensities across the entire spectrum was observed. The absorption features related to the minerals' O–H fundamental vibrations were maintained, such as those from gibbsite, kaolinite, vermiculite and goethite. Compared to clay minerals, the absorption features of quartz were the most affected by the addition of water due to the greater dispersion of this mineral caused by the increase of moisture (Janik et al., 2007).

Few researchers have reported common absorption features for water molecules in mid-IR spectra (Xia et al., 2018; Ma et al., 2019). The feature centered at 2450 cm^{-1} was wider for clay and narrower for sandy soil (Figs. 5 and 6). The contrasting behavior of both soils is related to their particle size distributions, structure and surface areas, which are much smaller for sand (quartz) compared to clay minerals (oxides and phyllosilicates) (Soriano-Disla et al., 2014). The soil pores are larger in the sandy soil and the water added to it is quickly absorbed, which gives the impression that it is wetter than the clay (Vepraskas, 1984). The soil components, such as oxides (mainly gibbsite) and OM, which were higher in the clay soil, tend to organize the particles on a microscopic scale (granular structure) (Ferreira et al., 1999). Thus, the water is mostly retained within the aggregate (macro and micro) (Saxton et al., 1986), which protects the water molecules from the incident radiation, causing less decrease in reflectance when compared to the sandy soil (Janik et al., 2016).

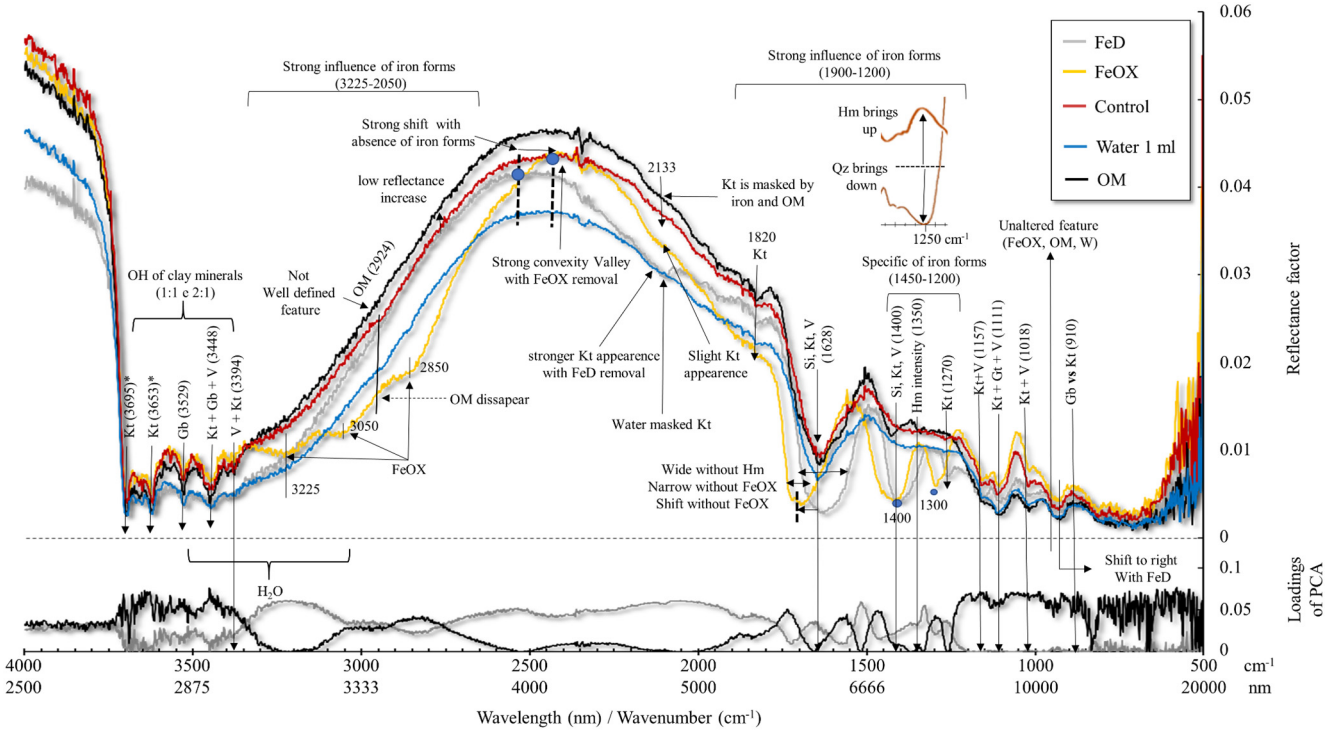

Fig. 6. Mid-IR spectra and loadings of Principal Components Analysis (PCA) to clay soil (Rhodic Hapludox). Control and removal treatments: OM, crystalline iron (FeD) and amorphous iron (FeOX) removals and spectra with addition of water (1 mL). Soil minerals and components are represented by the following acronyms: Gb: gibbsite, Hm: Hematite, Kt: kaolinite, OM: organic matter, Qz: quartz, Si: Silicon, V: vermiculite + mica.

3.4. Effects of OM removal

After removing the OM, the reflectance between 3500 cm^{-1} and 2000 cm^{-1} increased for both soils, although this effect was more evident in the sandy soil (Figs. 5 and 6). OḾs absorption features at 2924 cm^{-1} and 2843 cm^{-1} disappeared with this treatment in the sandy soil (Fig. 5). From 2000 to 500 cm^{-1}, OM also masked almost all mineraĺs diagnostic features reducing their intensities, such as the phyllosilicates and quartźs absorptions and reflection peaks, respectively in the clay and sandy soil (Figs. 5 and 6). At 1250 cm^{-1}, the OM removal revealed the effect of quartz coating by the amorphous iron in the sandy soil, where the quartźs reflection peaks (reststrahlen effects) were reduced instead of increasing due to influence of this masking (Fig. 5). The same effect was also observed to a lesser extent in the clay soil (Fig. 5). The OM removal from the clay soil showed previously hidden features, such as a reflection peak at 1500 cm^{-1}, due to kaolinite and amorphous iron as binding agent in aggregates. Also, we observe an absorption at 1425 cm^{-1}, due to the crystalline iron (hematite, in special), and another reflection peak at 1375 cm^{-1}, once more due to amorphous iron.

3.5. Effects of iron forms removal

The ammonium oxalate treatment is based on an acid solution, which extracts amorphous iron and maintains clay minerals and crystalline irons in the soil samples (hematite and goethite). The dithionite treatment destroys hematite and goethite plus amorphous irons, but does not extract other minerals such as kaolinite, montmorillonite, vermiculite and gibbsite. The removal of the irons forms (amorphous and crystalline) revealed how the mid-IR spectra have been influenced by the presence of these minerals, mainly affecting the reflectance intensities, absorption features, reflection peaks and masked other minerals in both soils (Figs. 5 and 6). Two main ranges with stronger influences were identified from 3225 to 2050 cm^{-1} and at 1200 cm^{-1}. The absorption features of gibbsite, phyllosilicates and quartz were not affected by the iron extraction, since most of them remained in both soiĺs spectral behavior (Figs. 5 and 6).

After amorphous iron removal, the Fe-OH stretching's absorption at 3448 cm^{-1} for goethite was maintained, and its other three features appeared at 3225, 2950, and 2870 cm^{-1} in both soils (Figs. 5 and 6). The last three absorptions are in agreement to those described from the goethite's pure spectrum (Clark et al., 2007). In the sandy soil, the amorphous iron removal destroyed the quartz coating and revealed the quartz's absorption features and reflection peaks from 2500 cm^{-1} to the end of the spectrum (Fig. 5). At 910 cm^{-1}, a gibbsite's absorption feature was highlighted by removing the amorphous iron. However, it appeared smaller (almost indistinguishable) in the control and OM-removing treatments. The absorption feature described occurred on the top of the kaolinite's reflection peak, suggesting similar proportions of both minerals.

In the clay soil, the kaolinite's absorption feature at 1820 cm^{-1} was probably masked by the hematite without the amorphous iron influence (Fig. 6). From 1690 cm^{-1} to the end of the spectrum, many absorptions and reflections features took place, which were earlier masked by the effects of OM and amorphous iron. The coincidence of high reflectance intensities due to hematite's reststrahlen effect probably induced a shift to the left of the features and peaks between 1690 cm^{-1} and 1225 cm^{-1}. Hematite affected the absorptions at 1690 cm^{-1}, 1425 cm^{-1}, and 1290 cm^{-1} and the reflections at 1550 cm^{-1} and 1350 cm^{-1}. At 1125 cm^{-1}, a kaolinite's reflection peak earlier masked by amorphous iron was shown. Despite the much higher content of gibbsite in the clay soil compared to the sandy one (Table 1), its absorption at 910 cm^{-1} was masked and gave way to the kaolinite's reflection peak in all treatments, since this phyllosilicate was more abundant in the clay fraction.

After crystalline iron removal, the goethite's absorptions at 3448 cm^{-1}, 3225 cm^{-1}, 2950 cm^{-1} and 2870 cm^{-1} were completely uncharacterized in both soil spectra, which confirmed the presence of this Fe oxide (Figs. 5 and 6). Overall, the absence of hematite and goethite also changed the soil spectral reflectance intensities, which

were considerably reduced in the beginning of the spectra (4000 cm^{-1} to 3100 cm^{-1}) and in the final range (1250 cm^{-1} to 500 cm^{-1}). However, the quartz and clay minerals' absorption features and peaks had been kept. In fact, a quartz's absorption at 2133 cm^{-1} was revealed in both spectra after the removal of crystalline iron, which suggested that it was masked by hematite. In the sandy soil, the reflectance intensities between 2600 cm^{-1} and 2080 cm^{-1} decreased after removing the influence of iron oxides without changing the quartz's features (Fig. 5). A reflection peak disappeared at 1650 cm^{-1}, and another at 1550 cm^{-1} was reduced and shifted to the right giving way to kaolinite. Both suggested the presence of hematite. In the clay soil, the removal of the crystalline iron increased the reflectance that previously had forced the displacement of the kaolinite's absorptions and reflections between 1690 cm^{-1} and 1225 cm^{-1}. These were eliminated by removing the hematite. The mentioned features were moved back to their original positions at 1640 cm^{-1}, 1410 cm^{-1}, and 1260 cm^{-1}, 1500 cm^{-1} and 1320 cm^{-1} (Fig. 6). Besides that, the hematite's reflection peak at 1225 cm^{-1} was remarkably reduced, becoming lower and giving way to the quartz's peak. The hematite's reflections at 1060 cm^{-1} and 1010 cm^{-1} also disappeared, besides the kaolinite's absorption at 1025 cm^{-1}. Thus, this study identified a new region of influence of hematite in the mid-IR spectrum, not as an absorption feature, but as an influence on the reflectance intensities.

3.6. Distinctions in the PCA environment

The PCA first two scores of the sandy and clay soil are shown in Fig. 7. The corresponding loadings are shown at the bottom of Figs. 5 and 6. For the clay soil, the first two PC explained almost 95% of the variance. For the sandy soil, the variance explained in the first PCA was half of that explained in the sandy soil. All treatments were very different, as observed by the distribution of point in both biplots (Fig. 7). The influence of water on the sandy soil was similar to the sample from which the crystalline iron removed, as the points in the biplot were very close. The points corresponding to the water and crystalline iron removal in the clay soil were well separated.

The loadings presented at the bottom of Figs. 5 and 6 showed the importance of each mid-IR band. The sandy and clay soils showed many differences in the loadings, since the most was between 3700 and 3000 cm^{-1} and around 600 cm^{-1} for the latter. Differently, for the sandy soil, the higher loadings were showed around 1500–1000 cm^{-1}, which is in accordance with the most important absorption features characteristic of quartz presence.

3.7. Correlation analysis

3.7.1. Laboratory spectra and soil attributes

The average mid-IR spectra of the seventeen control samples, with and without water addition, and their Pearson's correlation coefficients

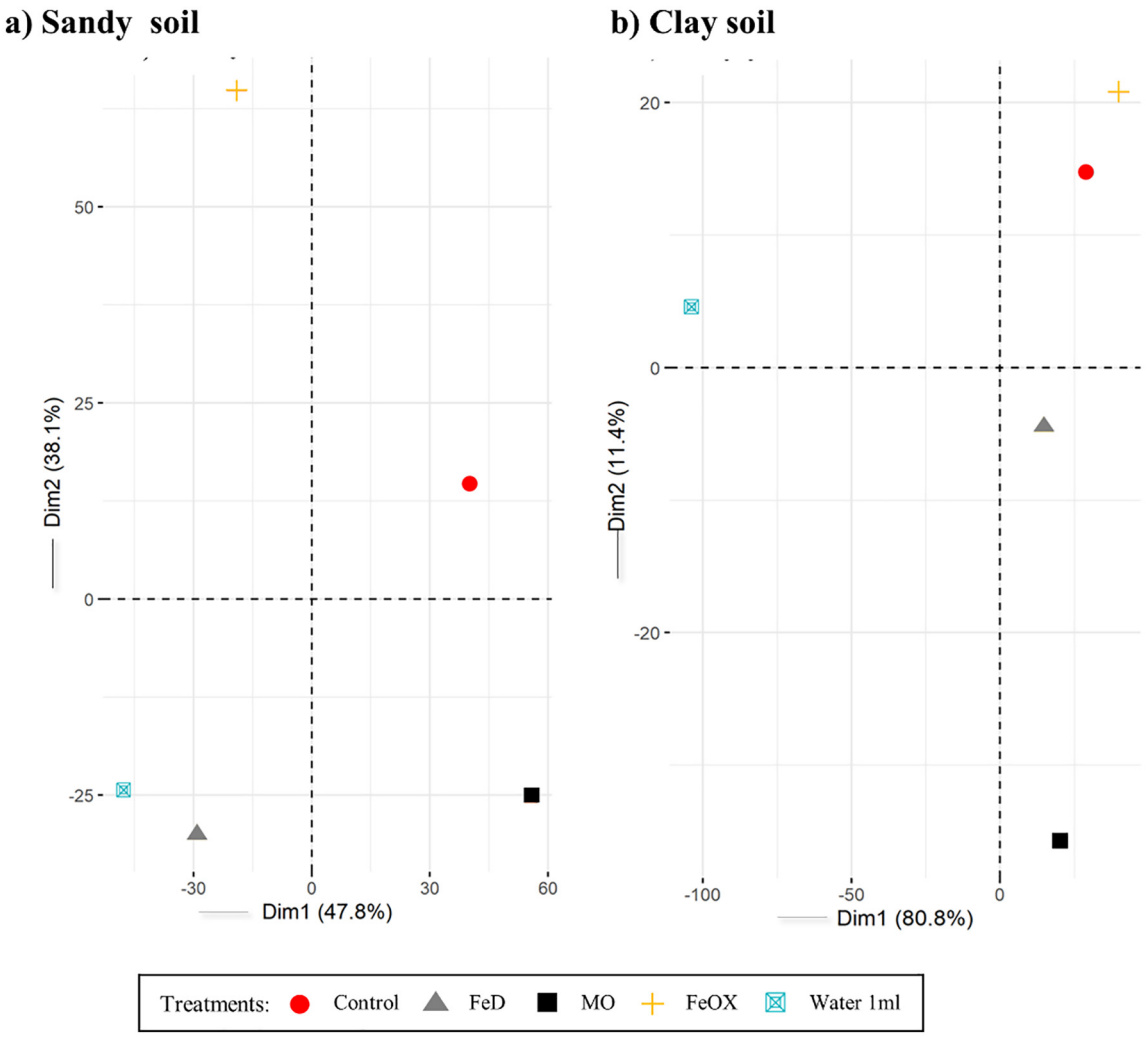

Fig. 7. Distribution of the PCA's scores for the control, OM, crystalline iron (FeD) and amorphous iron (FeOX) removal, and water (1 mL) treatments in mid-IR spectra of a) sandy (Typic Quartzpament) and b) clay (Rhodic Hapludox) soils.

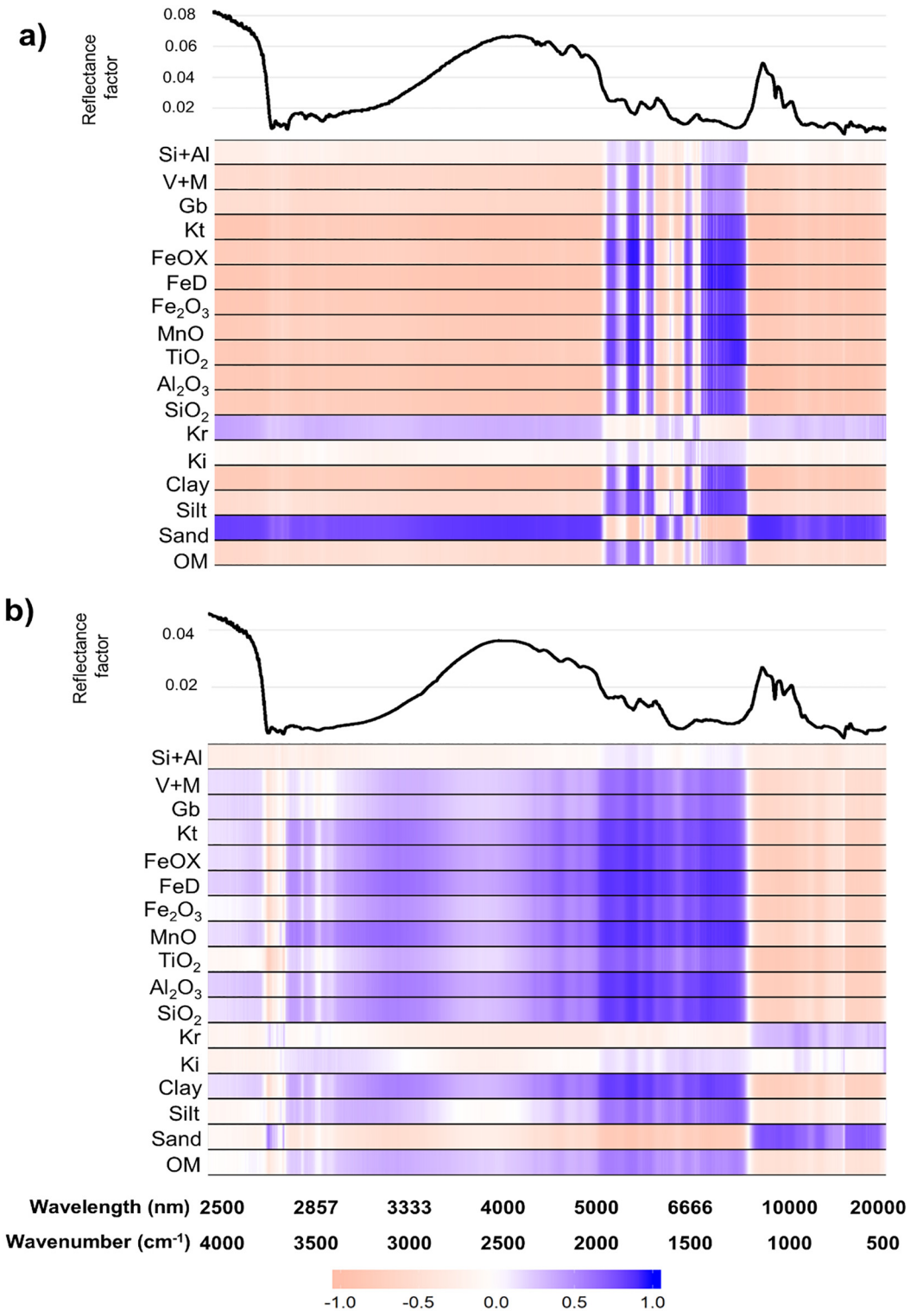

Fig. 8. Correlation plot between soil attributes and mid-IR spectra before (a) and after (b) the addition of water to the soil samples. Soil attributes are represented by the following acronyms: Si + Al: amorphous silica plus aluminium, V + M: vermiculites plus mica, GB: Gibbsite, Kt: Kaolinite, FeOX: amorphous iron, FeD: crystalline iron, Fe_2O_3: total iron, MnO: manganese oxide, TiO_2: titanium dioxide, Al_2O_3: aluminum oxide, SiO_2: silicon oxide, Kr and Ki: weathering index, OM: organic matter.

with soil attributes are shown (Fig. 8). The correlation coefficients were very different before and after the addition of water, mainly in the 4000–1200 cm^{-1}. The mid-IR spectra without water addition (Fig. 8a) showed mostly negative correlations with soil attributes, with exceptions to sand content, and ki and kr indices, which were highly positively correlated and poorly correlated with the spectra, respectively. In this region, the average mid-IR spectra, which received 1 mL, showed mostly positive correlation values for almost all soil attributes, with exceptions to ki and kr indices and sand content (Fig. 8b). Ki and Kr indices are used to describe the level of weathering of soils. They were calculated from iron and aluminum oxides, and are not spectrally active, which could be a possible reason for the low correlation

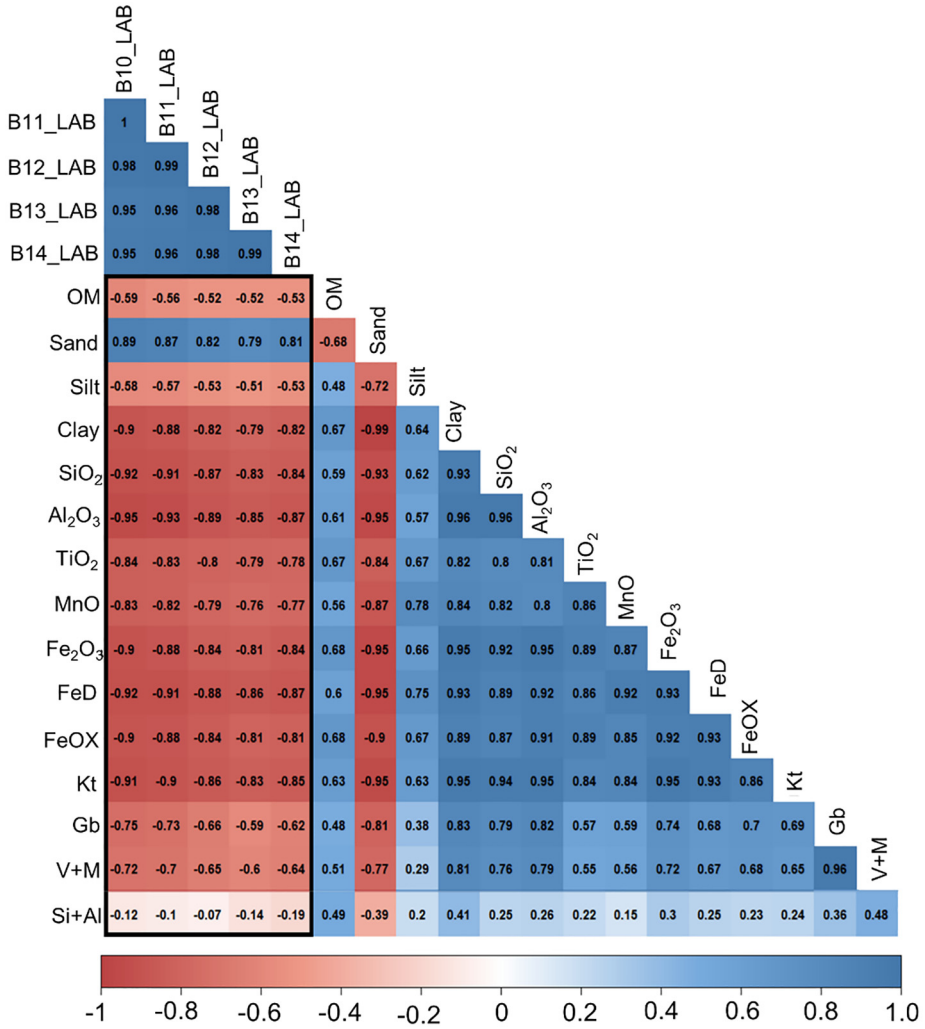

Fig. 9. Correlation matrix between ASTER simulated bands (B10_LAB, B11_LAB, B12_LAB, B13_LAB, and B14_LAB) and soil attributes. Soil attributes are represented by the following acronyms: Si + Al: amorphous silica plus aluminum, V + M: vermiculites plus mica, GB: Gibbsite, Kt: Kaolinite, FeOX: amorphous iron, FeD: crystalline iron, Fe_2O_3: total iron, MnO: manganese oxide, TiO_2: titanium dioxide, Al_2O_3: aluminum oxide, SiO_2: silicon oxide, Kr and Ki: weathering index, OM: organic matter.

coefficients observed. In wavenumbers > 1250 cm^{-1}, the correlation coefficients were very similar for both mid-IR spectra with and without water, although the correlation coefficients were slightly lower for the spectra in which the water was added. The spectral region above 1250 cm^{-1} corresponds to the thermal region of the spectrum. The sand correlation values in the thermal region were positive, which is in agreement with the results found by Salazar et al. (2020). In this region, strong Si-O asymmetric vibration occurs.

The correlation coefficients for mid-IR spectra without water addition and soil attributes were higher in 2000–1250 cm^{-1}, being positive correlations followed by negative correlations in a very short range of spectral bands (Fig. 8a). The mentioned pattern was not observed for the mid-IR spectra in which the water was added (Fig. 8b), in which the correlation coefficients were mostly positive.

The presence of water in soil samples can severely affect the spectral behavior in the mid-IR portion, more than in the other spectral ranges, as we observed also by the changes in correlation coefficients between spectra and soil attributes. It can also mask the absorption characteristic of some soil minerals (Chang et al., 2005). For kaolinite, Aghamir et al. (2019) observed that it was related to changes in spectra between 820 and 752 cm^{-1}. The authors also highlighted the absorption of quartz and clay in this range, reinforcing the fact that overlap may occur. Yitagesu et al. (2011) note that kaolinite showed asymmetric and sharply defined absorption minimum centered at ~ 3636.3 cm^{-1} and the absorption of a water molecule at ~ 1639.3 cm^{-1} decreased with increasing kaolinite content. Janik et al. (2016) found an inverse relationship to spectrum absorbance, in which they found a negative correlation between water and quartz, while clay had a positive correlation with soil moisture. Terra et al. (2015) observed that with the increase in water in the soil sample, sand and clay content presented an inverse behavior. The correlations coefficients between soil attributes and spectra with and without water highlighted the influence that water can has on soil minerals, making difficult their characterization or leading to wrong quantifications.

3.7.2. *ASTER satellite bands and soil attributes*

The relationship of soil attributes to the five ASTER satellite bands are shown (Fig. 9). The ASTER sensor covers the spectral region from 1250 to 714 cm^{-1} (8000 – 14000 nm), named as thermal infrared (TIR). Except for Si + Al content, whose correlation coefficient was low ($r < 0.2$), suitable results were obtained, mainly with mineralogical attributes, highlighting the potential of the ASTER sensor for the study of tropical soils. The correlation coefficients for all soil attributes were mainly negative, with exception to the sand content. The predominance of negative correlation coefficients is related to the fact that most of the studied minerals probably have strong absorption characteristics in this

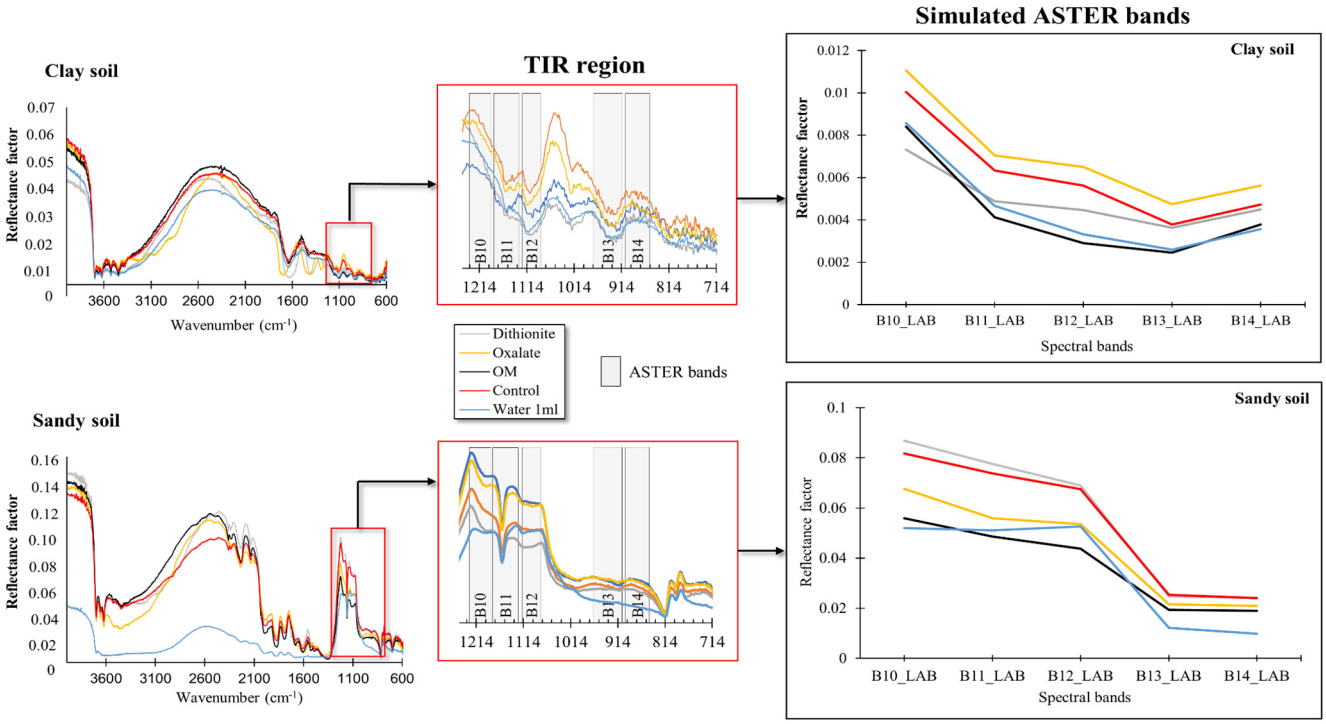

Fig. 10. Mid-IR and simulated ASTER bands of the sandy (Typic Quartzpament) and clayey (Rhodic Hapludox) soils. The red rectangle represents the thermal infrared region (TIR) covered by ASTER bands. Treatments are represented by the following acronyms: OM: organic matter removal, FeOX: amorphous iron removal, FeD: crystalline iron removal, and water (1 mL). (For interpretation of the references to colour in this figure legend, the reader is referred to the web version of this article.)

spectral region, which certainly decreases the reflectance values. The direct relationship (positive correlation) between the sand fraction and ASTER spectral bands refers to the low capacity of quartz to absorb radiation (Jović et al., 2019). The high correlation values with sand and clay indicate the high potential of the ASTER sensor for soil texture fractions determination. For the silt fraction, the correlation was low, probably due to the heterogeneity of minerals that make up this intermediate fraction and the way in this fraction is calculated from the clay and sand content difference.

High correlation values were also observed for Kt, Gb, V + M, SiO_2 and Fe_2O_3 (Fig. 9). These results highlighted the high potential of the ASTER sensor for distinguishing soil classes, since these mineralogical constituents are key soil attributes for soil classification. Such results suggest that future works should analyze the orbital information capacity, obtained by the ASTER sensor, in the characterization of physical and mineralogical attributes of tropical soils, and for soil classes' definition. The ASTER TIR bands can also be used to study weathering, depositional and erosional processes by using the mineralogical information. Cudahy et al. (2016), who tested the potential of using spectral indices calculated from ASTER TIR bands to study the processes mentioned also highlighted its importance.

In addition to mineralogical studies, ASTER bands were also used to obtain lithological information and suitable results were found for this application for almost twenty years (Abrams and Yamaguchi, 2019). Ninomiya et al. (2005), for example, studied the potential of ASTER bands to provided information about quartz, carbonates and silicate rocks by studying mineralogical indices. The indices can be obtained by simple map algebra between ASTER bands. The results obtained in this work can be used to improve to improve the mineralogical indices already in use. In this sense, Breunig et al. (2009) used ASTER bands B10 and B14 ratio to study the presence of quartz, which is related to the sand fraction. In our study, the correlation between sand fraction and simulated ASTER bands B10 and B14 was up to 0.8. In addition, another strong relation between different bands in the TIR region and the studied minerals was observed, which shows that reflectance in this region could simulate the variations that occur in the soil composition (Fig. 9).

The mid-IR spectra and the ASTER simulated bands for sandy and clay soils are shown in Fig. 10. Although it is interesting to consider the potential of satellite bands in the soil minerals study, the main issue is that only thermal bands in the 1250 – 714 cm^{-1} (8000 – 14000 nm) spectral range are considered, which does not allow a better study of the mineral absorption features in other regions. The ASTER simulated spectral bands were very different for both soils and are in agreement with Salazar et al. (2020), who characterized soil texture by ASTER images. The simulated bands for sandy soil best represented the absorption feature shown in the original laboratory spectra, characteristics of quartz minerals. The lab spectra from clay soil showed high variability in this region, which was difficult to distinguish with simulated ASTER bands. It was also observed that in sandy soil the ASTER simulated bands showed convex behavior in the shape of the curves, while in clay soil the concave shape predominates, in agreement with Salazar et al. (2020). The agreement with the indicated authors makes strong the simulation of the present spectra in the laboratory and confirms the importance of these controlled experiments for further image interpretation.

3.8. New bands suggestions in the mid-IR range

Considered as useful tools for geological mapping and minerals explorations (Abrams and Yamaguchi, 2019; Bhadra et al., 2013; Cudahy et al., 2016; Fu et al., 2019; Kurata and Yamaguchi, 2019), simulated TIR bands have been successfully tested to discriminate contrasting soils in this study (Fig. 9). However, the use of remote sensing images is limited by the influence of several atmospheric factors (Ben-Dor et al., 2009), which sometimes limit the definition of spectral regions useful for mineralogical studies. For example, the highest atmospheric attenuation in the mid-IR portion is between 740 and

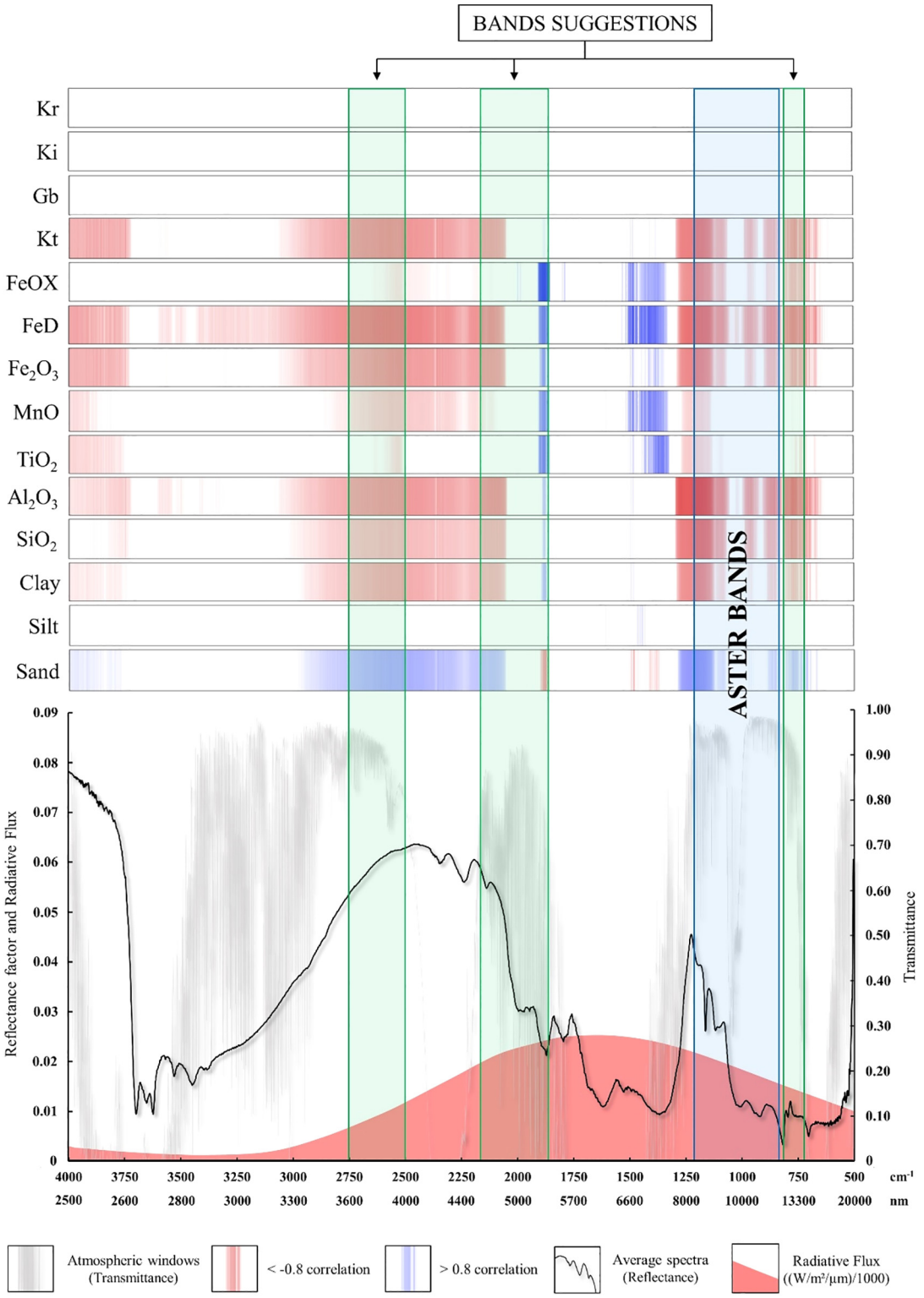

Fig. 11. Spectral ranges for possible bands suggestions of future sensors in the mid-IR, according to high correlations values. Soil attributes are represented by the following acronyms: Si + Al: amorphous silica plus aluminum, V + M: vermiculites plus mica, GB: Gibbsite, Kt: Kaolinite, FeOX: amorphous iron, FeD: crystalline iron, Fe_2O_3: total iron, MnO: manganese oxide, TiO_2: titanium dioxide, Al_2O_3: aluminum oxide, SiO_2: silicon oxide, Kr and Ki: weathering index, OM: organic matter.

625 cm^{-1} (13000 – 16000 nm) and at 1050 cm^{-1} (9500 nm). Atmospheric absorption also occurs at 1000 cm^{-1} (10000 nm), mainly due to the presence of carbon dioxide, methane, water vapor and ozone in the atmosphere. Besides the atmospheric windows, another problem of great importance for the definition of passive orbital sensor bands is the low solar radiative flux in the initial mid-IR range (4000 to 3000 cm^{-1} or 2500 – 3300 nm). For this reason, it is not possible to deploy bands in orbital sensors to obtain information from the range mentioned. Therefore, only the thermal range is used, because in this band, instead of the sun, it is the earth that radiates energy to the sensor by heat waves. Considering all the factors involved, we defined three cumulative filters to identify important regions for the inclusion of bands in

future satellite sensors: I) high correlations regions between mid-IR spectra and soil attributes; II) atmospheric windows regions; and III) high radiative flux. The use of these cumulative filters provided the identification of three spectral regions with high potential for bands inclusion in orbital sensors, highlighted in Fig. 11.

First, it is important to stress that the ASTER bands were located in a region with high correlation values between soil attributes and spectral information. Besides, it was possible to highlight three new regions, with coincidences of high correlation values, high radiative flux and atmospheric windows: 2760 – 2500 cm^{-1} (3600 – 4000 nm), 2150 – 1875 cm^{-1} (4600 – 5300 nm) and 840 – 740 cm^{-1} (11900 – 3500 nm). It is of great importance that new regions of high correlations be considered, with the aim to increase the potential use of orbital sensors for several environmental applications. For example, the ASTER bands present few wavenumbers highly correlated with TiO_2 and MnO_2 (manganese dioxide), in the region between 2150 and 1875 cm^{-1} (4600 – 5300 nm), proposed here as a new spectral band. In addition, Kr, Ki and gibbsite do not showed correlation coefficients above the threshold (> 0.8 or < -0.8). We suggest that future studies analyze other soil attributes to reinforce the potential of new regions proposed here to complement the existing bands in orbital sensors.

4. Conclusions and final remarks

The mid-IR spectral behaviors of different soils under influence of water, organic matter and iron forms (amorphous and crystalline) were evaluated. The clay and sandy soils present several differences in their spectral behavior i.e., on reflectance intensity, spectral features, reflectance peaks, and specific shapes. Soil moisture masks features and decreases reflectance intensities, but soil mineral characteristics are still maintained. OM decreases reflectance intensities in 4000 – 2000 cm^{-1}. The sandy soil shows greater disturbance in reflectance intensity and features/peaks of the mid-IR region when moistened or with OM removal.

The clay soil presents severe alteration in the absorption features after the iron forms removal. Amorphous iron alters spectra in several ways, masking some silicate's features (quartz and kaolinite) and reducing the reflectance intensities. This type of iron did not present any features but it interferes on the reflectance intensity of other minerals, such as quartz and kaolinite. Crystalline irons acts in both, absorption features and reflectance intensity in several parts of the spectrum. The balanced forces seems complex and needs further experiments. This study was able to identify the influence of hematite not based on its characteristic absorption features, but on its reflectance intensities in soil mid-IR spectra.

The mid-IR region showed high accuracy for the mineralogy and physical attributes prediction of the tropical soils. High correlation values were observed between Kt, Gb, SiO_2, Fe_2O_3 and ASTER bands. Although ASTER bands showed potential to soil mineralogical studies, only a small region of the mid-IR lab spectra is covered for this sensor (thermal portion), which sometimes can fail to accurately describe soil mineralogy. The spectral bands proposed (2760 to 2500 cm^{-1}, 2150 to 1875 cm^{-1}, and 840 to 740 cm^{-1}) showed good correlation with soil minerals and can assist forthcoming satellites, which will cover mid-IR spectral range.

The complexity of interaction and influence of OM and iron forms are evident, and indicate the necessity for future analysis to better understanding of their impacts on soil mid-IR spectra.

Declaration of Competing Interest

The authors declare that they have no known competing financial interests or personal relationships that could have appeared to influence the work reported in this paper.

Acknowledgments

We would like to thank the National Scholarship Program "Don Carlos Antonio López" (BECAL) of the Government of Paraguay for granting the scholarship to the first author. To the São Paulo Research Foundation (FAPESP) for the financial support (Project grant n. 2014/22262-0). To the Geotechnologies on Soil Science group - GeoCIS (*esalqgeocis.wixsite.com/english*) and to everybody that directly or indirectly assisted on publishing this study.

Appendix A. Supplementary data

Supplementary data to this article can be found online at https://doi.org/10.1016/j.geoderma.2020.114480.

References

Abrams, M., Yamaguchi, Y., 2019. Twenty years of ASTER contributions to lithologic mapping and mineral exploration. Remote Sens. https://doi.org/10.3390/rs11111394.

Aghamir, F., Hamidi, S.M., Tehranchi, M.M., Mirzaiee, R., 2019. Combined Application of Imaging Methods for Estimating Soil Physicochemical Properties. Eurasian Soil Sci. 52, 926–934. https://doi.org/10.1134/s1064229319080027.

Bahia, A.S.R. de S., Marques, J., Siqueira, D.S., 2015. Procedures using diffuse reflectance spectroscopy for estimating hematite and goethite in Oxisols of São Paulo, Brazil. Geoderma Reg. 5, 150–156. https://doi.org/10.1016/j.geodrs.2015.04.006.

Ben-Dor, E., Chabrillat, S., Demattê, J.A.M.A.M., Taylor, G.R.R., Hill, J., Whiting, M.L.L., Sommer, S., 2009. Using Imaging Spectroscopy to study soil properties. Remote Sens. Environ. 113, S38–S55. https://doi.org/10.1016/j.rse.2008.09.019.

Bhadra, B.K., Pathak, S., Karunakar, G., Sharma, J.R., 2013. ASTER Data Analysis for Mineral Potential Mapping Around Sawar-Malpura Area, Central Rajasthan. J. Indian Soc. Remote Sens. 41, 391–404. https://doi.org/10.1007/s12524-012-0237-0.

Breunig, F.M., Galvão, L.S., Formaggio, A.R., Couto, E.G., 2009. The combined use of reflectance, emissivity and elevation Aster/Terra data for tropical soil studies. Rev. Bras. Ciência do Solo 33, 1785–1794. https://doi.org/10.1590/s0100-06832009000600027.

Chang, C.-W., Laird, D.A., Hurburgh, C.R., 2005. Influence of soil moisture on near-infrared reflectance spectroscopic measurement of soil properties. Soil Sci. 170, 244–255. https://doi.org/10.1097/01.ss.0000162289.40879.7b.

Chen, J., Anandarajah, A., Inyang, H., 2000. Pore fluid properties and compressibility of kaolinite. J. Geotech. Geoenvironmental Eng. 126, 798–807.

Clark, R.N., Swayze, G.A., Wise, R.A., Livo, K.E., Hoefen, T.M., Kokaly, R.F., Sutley, S.J., 2007. USGS Digital Spectral Library splib06a, U. S. Geological Survey. https://doi.org/10.3133/DS231.

Cudahy, T., Caccetta, M., Thomas, M., Hewson, R., Abrams, M., Kato, M., Kashimura, O., Ninomiya, Y., Yamaguchi, Y., Collings, S., Laukamp, C., Ong, C., Lau, I., Rodger, A., Chia, J., Warren, P., Woodcock, R., Fraser, R., Rankine, T., Vote, J., De Caritat, P., English, P., Meyer, D., Doescher, C., Fu, B., Shi, P., Mitchell, R., 2016. Satellite-derived mineral mapping and monitoring of weathering, deposition and erosion. Sci. Rep. 6, 1–12. https://doi.org/10.1038/srep23702.

Demattê, J.A.M., Bellinaso, H., Romero, D.J., Fongaro, C.T., 2014. Morphological Interpretation of Reflectance Spectrum (MIRS) using libraries looking towards soil classification. Sci. Agric. 71, 509–520. https://doi.org/10.1590/0103-9016-2013-0365.

Demattê, J.A.M., Nanni, M.R., Formaggio, A.R., Epiphanio, J.C.N., 2007. Spectral reflectance for the mineralogical evaluation of Brazilian low clay activity soils. Int. J. Remote Sens. 28, 4537–4559. https://doi.org/10.1080/01431160701250408.

EMBRAPA, 1997. Manual de Métodos de Análise de Solo, 5a. ed. UFLA, LAVRAS.

Fang, Q., Hong, H., Zhao, L., Kukolich, S., Yin, K., Wang, C., 2018. Visible and Near-Infrared reflectance spectroscopy for investigating soil mineralogy: A review. J. Spectrosc. https://doi.org/10.1155/2018/3168974.

Farmer, V.C., 1968. Infrared spectroscopy in clay mineral studies. Clay Miner. 7, 373–387.

Ferreira, M.M., Fernandes, B., Curi, N., 1999. Mineralogia da fração argila e estrutura de latossolos da região sudeste do Brasil. Rev. Bras. Ciência do Solo 23, 507–514. https://doi.org/10.1590/s0100-06831999000300003.

Fu, H., Fu, B., Ninomiya, Y., Shi, P., 2019. New Insights of Geomorphologic and Lithologic Features on Wudalianchi Volcanoes in the Northeastern China from the ASTER Multispectral Data. Remote Sens. 11, 2663. https://doi.org/10.3390/rs11222663.

Gholoubi, A., Emami, H., Jones, S.B., Tuller, M., 2018. A Novel Shortwave Infrared Proximal Sensing Approach to Quantify the Water Stability of Soil Aggregates. Soil Sci. Soc. Am. J. 82, 1358. https://doi.org/10.2136/sssaj2018.05.0170.

Holmgren, G.G.S., 1967. A Rapid Citrate-Dithionite Extractable Iron Procedure. Soil Sci. Soc. Am. Proc. 31, 210–221.

Jackson, M.L., 1969. Soil Chemical Analysis. Advanced Course.

Janik, L.J., Merry, R.H., Forrester, S.T., Lanyon, D.M., Rawson, A., 2007. Rapid prediction of soil water retention using mid infrared spectroscopy. Soil Sci. Soc. Am. J. 71, 507–514. https://doi.org/10.2136/sssaj2005.0391.

Janik, L.J., Soriano-Disla, J.M., Forrester, S.T., McLaughlin, M.J., 2016. Moisture effects on diffuse reflection infrared spectra of contrasting minerals and soils: A mechanistic

interpretation. Vib. Spectrosc. 86, 244–252. https://doi.org/10.1016/J.VIBSPEC.2016.07.005.
Jović, B., Ćirić, V., Kovačević, M., Šeremešić, S., Kordić, B., 2019. Empirical equation for preliminary assessment of soil texture. Spectrochim. Acta - Part A Mol. Biomol. Spectrosc. 206, 506–511. https://doi.org/10.1016/j.saa.2018.08.039.
Kurata, K., Yamaguchi, Y., 2019. Integration and Visualization of Mineralogical and Topographical Information Derived from ASTER and DEM Data. Remote Sens. 11, 162. https://doi.org/10.3390/rs11020162.
Laub, M., Blagodatsky, S., Nkwain, Y.F., Cadisch, G., 2019. Soil sample drying temperature affects specific organic mid-DRIFTS peaks and quality indices. Geoderma 355, 113897. https://doi.org/10.1016/J.GEODERMA.2019.113897.
Laukamp, C., Caccetta, M., Collings, S., Cudahy, T., Thomas, M., Ong, C., Haest, M., 2012. Continent-scale mineral information from ASTER multispectral satellite data, in: International Geoscience and Remote Sensing Symposium (IGARSS). IEEE, pp. 7553–7556. https://doi.org/10.1109/IGARSS.2012.6351883.
Ma, F., Du, C.W., Zhou, J.M., Shen, Y.Z., 2019. Investigation of soil properties using different techniques of mid-infrared spectroscopy. Eur. J. Soil Sci. 70, 96–106. https://doi.org/10.1111/ejss.12741.
Madejová, J., 2003. FTIR techniques in clay mineral studies. Vib. Spectrosc. https://doi.org/10.1016/S0924-2031(02)00065-6.
Madejová, J., Gates, W.P., Petit, S., 2017. IR Spectra of Clay Minerals, in: Developments in Clay Science. Elsevier B.V., pp. 107–149. https://doi.org/10.1016/B978-0-08-100355-8.00005-9.
McDowell, M.L., Bruland, G.L., Deenik, J.L., Grunwald, S., Knox, N.M., 2012. Soil total carbon analysis in Hawaiian soils with visible, near-infrared and mid-infrared diffuse reflectance spectroscopy. Geoderma 189–190, 312–320. https://doi.org/10.1016/j.geoderma.2012.06.009.
McKeague, J.A., Day, J.H., 1965. Dithionite and oxalate extractable Fe and Al as aids in differentiating various class of soils. Can. J. Soil Sci. 46, 13–22.
Mulder, V.L., de Bruin, S., Weyermann, J., Kokaly, R.F., Schaepman, M.E., 2013. Characterizing regional soil mineral composition using spectroscopy and geostatistics. Remote Sens. Environ. 139, 415–429. https://doi.org/10.1016/j.rse.2013.08.018.
Nguyen, T.T., Janik, L.J., Raupach, M., 1991. Diffuse reflectance infrared fourier transform (Drift) spectroscopy in soil studies. Aust. J. Soil Res. 29, 49–67. https://doi.org/10.1071/SR9910049.
Niemeyer, J., Chen, Y., Bollag, J.M., 1992. Characterization of humic acids, composts, and peat by diffuse reflectance Fourier-transform infrared spectroscopy. Soil Sci. Soc. Am. J. 56, 135–140. https://doi.org/10.2136/sssaj1992.03615995005600010021x.
Ninomiya, Y., Fu, B., 2019. Thermal infrared multispectral remote sensing of lithology and mineralogy based on spectral properties of materials. Ore Geol. Rev. https://doi.org/10.1016/j.oregeorev.2018.03.012.
Ninomiya, Y., Fu, B., Cudahy, T.J., 2005. Detecting lithology with Advanced Spaceborne Thermal Emission and Reflection Radiometer (ASTER) multispectral thermal infrared “radiance-at-sensor” data. Remote Sens. Environ. 99, 127–139. https://doi.org/10.1016/j.rse.2005.06.009.
R Core Team, 2019. R: A language and environment for statistical computing. R Foundation for Statistical Computing, Vienna, Austria. https://www.R-project.org/.
Robotti, N., 2013. The discovery of X-ray diffraction. Rend. Fis. Acc. Lincei 24, S7–S18. https://doi.org/10.1007/s12210-012-0205-1.
Salazar, D.F.U., Demattê, J.A.M., Vicente, L.E., Guimarães, C.C.B., Sayão, V.M., Cerri, C.E.P., Manuela, M.C., Mendes, W.D.S., 2020. Emissivity of agricultural soil attributes in southeastern Brazil via terrestrial and satellite sensors. Geoderma 361, 114038. https://doi.org/10.1016/j.geoderma.2019.114038.
Salisbury, J., 1988. Mid-Infrared (2.1-2.5 um) Spectra of MInerals. Second edition.
Salisbury, J.W., 1987. Mid-Infrared (2.1-25 urn) Spectra of Minerals. First Edition.
Salisbury, J.W., D’Aria, D.M., 1992. Emissivity of terrestrial materials in the 8–14 μm atmospheric window. Remote Sens. Environ. 42, 83–106. https://doi.org/10.1016/0034-4257(92)90092-X.
Salisbury, J.W., Eastes, J.W., 1985. The effect of particle size and porosity on spectral contrast in the mid-infrared. Icarus 64, 586–588. https://doi.org/10.1016/0019-1035(85)90078-8.
Santos, H.G., Jacomine, P.K.T., Anjos, L.H.C., Oliveira, V.A., Oliveira, J.B., Coelho, J.F., Cunha, T.J.F., 2013. Sistema brasileiro de classificação de solos, Embrapa Solos. https://doi.org/ISBN 978-85-7035-198-2.
Saxton, K.E., Rawls, W.J., Romberger, J.S., Papendick, R.I., 1986. Estimating generalized soil-water characteristics from texture. Soil Sci. Soc. Am. J. 50, 1031–1036. https://doi.org/10.2136/sssaj1986.03615995005000040039x.
Schaefer, C.E.G.R., Fabris, J.D., Ker, J.C., 2008. Minerals in the clay fraction of Brazilian Latosols (Oxisols): a review. Clay Miner. 43, 137–154. https://doi.org/10.1180/claymin.2008.043.1.11.
Smalley, I.J., Cabrera, J.G., 1969. Particle association in compacted kaolinite. Nature. https://doi.org/10.1038/222080a0.
Soil Survey Staff, 2014. Claves para la Taxonomía de Suelos., Decima seg. ed. NRCS - USDA.
Soriano-Disla, J.M., Janik, L.J., Viscarra Rossel, R.A., MacDonald, L.M., McLaughlin, M.J., 2014. The performance of visible, near-, and mid-infrared reflectance spectroscopy for prediction of soil physical, chemical, and biological properties. Appl. Spectrosc. Rev. https://doi.org/10.1080/05704928.2013.811081.
Stenberg, B., Viscarra Rossel, R.A., Mouazen, A.M., Wetterlind, J., 2010. Visible and Near Infrared Spectroscopy in Soil Science. Adv. Agron. 107, 163–215. https://doi.org/10.1016/S0065-2113(10)07005-7.
Stumpe, B., Weihermuller, L., Marschner, B., 2011. Sample preparation and selection for qualitative and quantitative analyses of soil organic carbon with mid-infrared reflectance spectroscopy. Eur. J. Soil Sci. 62, 849–862.
Sun, W., Zhang, X., Sun, X., Sun, Y., Cen, Y., 2018. Predicting nickel concentration in soil using reflectance spectroscopy associated with organic matter and clay minerals. Geoderma 327, 25–35. https://doi.org/10.1016/j.geoderma.2018.04.019.
Teixeira, P.C., Donagema, G.K., Fontana, A., Teixeira, W.G., 2017. Manual de Métodos de Análise. de Solo.
Terra, F.S., Demattê, J.A.M., Viscarra Rossel, R.A., 2015. Spectral libraries for quantitative analyses of tropical Brazilian soils: Comparing vis-NIR and mid-IR reflectance data. Geoderma 255–256, 81–93. https://doi.org/10.1016/j.geoderma.2015.04.017.
Thomson, J.L., Salisbury, J.W., 1993. The mid-infrared reflectance of mineral mixtures (7–14 μm). Remote Sens. Environ. 45, 1–13. https://doi.org/10.1016/0034-4257(93)90077-B.
Tsu, H., Yamaguchi, Y., Kahle, A.B., 1996. ASTER science mission overview, in: S. Scholl, M., Andresen, B.F. (Eds.), Infrared Spaceborne Remote Sensing IV. SPIE, p. 52. https://doi.org/10.1117/12.255200.
Vepraskas, M.J., 1984. Cone index of loamy sands as influenced by pore size distribution and affective stress. Soil Sci. Soc. Am. J. 48, 1220–1225. https://doi.org/10.2136/sssaj1984.03615995004800060003x.
Vicente, L.E., de Souza Filho, C.R., 2011. Identification of mineral components in tropical soils using reflectance spectroscopy and advanced spaceborne thermal emission and reflection radiometer (ASTER) data. Remote Sens. Environ. 115, 1824–1836.
Viscarra Rossel, R.A., Walvoort, D.J.J., McBratney, A.B., Janik, L.J., Skjemstad, J.O., 2006. Visible, near infrared, mid infrared or combined diffuse reflectance spectroscopy for simultaneous assessment of various soil properties. Geoderma 131, 59–75. https://doi.org/10.1016/j.geoderma.2005.03.007.
Walkley, A., Black, I.A., 1934. An examination of the Degtjareff method for determining soil organic matter, and a proposed modification of the chromic acid titration method. Soil Sci. 37, 29–38.
White, J.L., Roth, C.B., 1986. Infrared Spectrometry, in: Klute, A. (Ed.), Methods of Soil Analysis: Part 1. Physical and Mineralogical Methods. ASA, Madison, pp. 291–330. https://doi.org/10.2136/sssabookser5.1.2ed.c11.
Wille, F., Nehrig, M., Feldkamp, M., 2015. Thermal performance of transportation packages for radioactive materials, in: Safe and Secure Transport and Storage of Radioactive Materials. Elsevier Inc., pp. 107–121. https://doi.org/10.1016/B978-1-78242-309-6.00008-3.
Xia, Y., Ugarte, C.M., Guan, K., Pentrak, M., Wander, M.M., 2018. Developing Near- and Mid-Infrared Spectroscopy Analysis Methods for Rapid Assessment of Soil Quality in Illinois. Soil Sci. Soc. Am. J. 82, 1415. https://doi.org/10.2136/sssaj2018.05.0175.
Yeasmin, S., Singh, B., Johnston, C.T., Sparks, D.L., 2017. Evaluation of pre-treatment procedures for improved interpretation of mid infrared spectra of soil organic matter. Geoderma 304, 83–92. https://doi.org/10.1016/J.GEODERMA.2016.04.008.
Ziechmann, W., 1964. Spectroscopic investigations of lignin, humic substances and peat. Geochim. Cosmochim. Acta 28, 1555–1566. https://doi.org/10.1016/0016-7037(64)90006-7.